Transmission electron microscopy microstructural characterization of Ti–Si–C–N coatings

Guo, Y; Ma, S; Xu, K; Bell, Thomas; Li, Xiao-Ying; Dong, Hanshan

DOI:
10.1557/jmr.2008.0019

Transmission electron microscopy microstructural characterization of Ti–Si–C–N coatings

Yan Guo, Shengli Ma, and Kewei Xu
International Surface Engineering Research & Development Centre, Xi'an Jiaotong University, China

Tom Bell
International Surface Engineering Research & Development Centre, Xi'an Jiaotong University, China; and Department of Metallurgy and Materials, The University of Birmingham, Birmingham B15 2TT, United Kingdom

Xiaoying Li and Hanshan Dong[a)]
Department of Metallurgy and Materials, The University of Birmingham, Birmingham B15 2TT, United Kingdom

(Received 21 May 2007; accepted 25 September 2007)

A new type of Ti–Si–C–N coatings deposited on high-speed steel substrate by means of pulsed direct current (dc) plasma-enhanced chemical vapor deposition was investigated. The as-deposited coatings were characterized systematically by using energy-dispersive x-ray spectroscopy, x-ray diffraction (XRD), transmission electron microscopy (TEM), and microhardness with particular attention paid to the microstructure of the coatings. It has been shown that C content has a profound effect on the microstructure and hardness of coatings. TEM and XRD analyses revealed that these coatings consist of the dominate Ti(C, N) with a silicide ($TiSi_2$, Si_3N_4, or SiC, depending on the C content in the coatings). The crystallite sizes are in the range of 8–35 nm, which decrease with increasing C content. The Ti–Si–C–N coatings with high C content (25.2–38.6 at.%) possess superhardness (41–48 GPa). This can be attributed to the grain refinement/grain boundary hardening and dispersion hardening of the hard, nanosized crystalline Si_3N_4 or SiC formed in the deposition.

I. INTRODUCTION

Due to such attractive properties as high hardness, good wear resistance, and chemical stability, binary hard coatings such as TiN have been successfully used to increase the lifetime and performance of cutting tools, dies and molds, and many other engineering components.[1,2] However, TiN coatings are not suitable for high-temperature (>500 °C) applications because of their poor oxidation resistance,[3,4] as well as for heavy-load applications under contact conditions.

Therefore, great efforts have been made to develop new hard coatings based on ternary Ti–X–N systems (where X = B, C, Al, Si, Cr, etc.) to further improve hardness, wear, and oxidation resistance.[5–9] For example, some researchers have found that superhardness (>40 GPa) and excellent oxidation resistance (>1000 °C) can be achieved from such ternary coating systems as Ti–Si–N, Ti–B–N, and Ti–Al–N.[9–11] However, these superhard coatings are characterized by high friction coefficients (0.60–0.75),[12,13] which has restricted them to cutting-tool applications. To this end, some researchers have explored a new quaternary system, Ti–Si–C–N, and superhardness (55 GPa) combined with a relatively low friction coefficient (0.50) has been achieved.[14] This could pave the way for diverse applications of such very promising superhard coatings.

Notwithstanding the fact that detailed process–property relationships have been established based on systematic experimental work, the microstructure characterization and thus the understanding of the hardening mechanism involved are well behind process studies. Indeed, the microstructure and in particular the state (crystalline or amorphous) of Si_3N_4 is still a topic open to debate because the amount and the size of the Si_3N_4 phase may be below the detection limit of x-ray diffraction (XRD) analysis. For instance, some previous research claimed that Si_3N_4 phase is amorphous because x-ray photoelectron spectroscopy (XPS) proved the existence of the Si_3N_4 phase, but XRD did not show crystalline Si_3N_4 peaks. It should be noted that, without detailed direct transmission electron microscopy (TEM)

a)Address correspondence to this author.
e-mail: h.dong.20@bham.ac.uk
DOI: 10.1557/JMR.2008.0019

studies, it is difficult—if not impossible—to interpret the state of secondary phases such as Si_3N_4.[15]

Accordingly, in this investigation a series of quaternary Ti–Si–C–N coatings were synthesized using the pulsed direct current (dc) plasma-enhanced chemical vapor deposition (PECVD) method due to the fact that PECVD has good coverage characteristics and is thus suitable for complex-shaped tools and dies. Detailed TEM microstructural characterization has been conducted in conjunction with XRD and nanoindentation to advance scientific understanding of the microstructure, the microstructure–hardness relationship, and thus the hardening mechanisms involved.

II. EXPERIMENTAL

Quaternary Ti–Si–C–N coatings were deposited on a high-speed steel (HSS) substrate by pulsed dc PECVD for surface microstructural studies. A schematic diagram of the PECVD deposition system has been shown elsewhere.[1,2] Prior to deposition, the HSS substrate was cleaned in the deposition chamber by ion etching with H^+ and Ar^+ ions for 30 min to remove the surface oxides. During deposition, the substrate temperature was kept at about 550 °C, the pressure was kept at 200 Pa, and the deposition time was 4 h. $TiCl_4$, $SiCl_4$, N_2, H_2, and Ar were used as reactant gases at a gas flow rate of 20, 8, 400, 800, and 50 mL/min, respectively. CH_4 flow rate was adjusted from 60 to 320 mL/min (see Table I) to prepare coatings with different carbon contents. The flow rate of the different gases was measured and controlled by mass flow controllers. $TiCl_4$ was led into the chamber from the $TiCl_4$ tank at a constant temperature of 40 °C, and $SiCl_4$ was led into chamber from the $SiCl_4$ tank at room temperature.

Coating compositions were analyzed by energy-dispersive x-ray spectroscopy (EDX) attached to the JSM6460 (JEOL, Tokyo, Japan) scanning electron microscopy (SEM) instrument, under 20 kV. Hardness was measured by a Fischerscope 100 (Sinddelfingen, Maichingen, Germany) under a load of 5 g using a Vickers diamond indenter. The indention depth was controlled within 5%–10% of the coating thickness to avoid the substrate effect on the hardness value measured, and five repeated measurements were conducted and the average value reported. A D/max-3C x-ray Rigaku (Tokyo, Japan) diffractometer (XRD) with Cu K_α radiation was used to identify crystal structure and orientation of the coatings. The voltage, current, step size, and sampling time used in the XRD were 40 kV, 40 mA, 0.02°, and 1 s, respectively.

TEM samples were prepared as follows. A foil about 500 μm thick was cut parallel to the treated surface and mechanically ground to a thickness of 40 μm, from which TEM disks of 3 mm in diameter were punched. Single-jet electropolishing was performed using a 10% perchloric acid/90% acetic acid solution at room temperature, with a polishing current of 30 mA. TEM observations were carried out in a Philips CM20 TEM (Philips/FEI, Eindhoven, The Netherlands) operating at 200 kV.

III. RESULTS AND DISCUSSION

A. Composition analysis

Table I shows the composition of Ti–Si–C–N coatings as a function of CH_4 flow rates. It can be seen that C content increased and N content decreased linearly with CH_4 flow rate in the range of 10.2–38.6 and 13.4–38.5 at.%, respectively; however, there is no evident correlation between the content of Ti, Si, O, or Cl with CH_4 flow rate. The most likely source of oxygen was from residual oxygen in the deposition chamber.

B. XRD characterization

Fig. 1 shows the XRD patterns of HSS substrate and five coatings with different C contents. It can be seen that a set of peaks with the diffraction angles between TiC and TiN were identified for all coatings. However, coatings with low C content, such as 14.0 and 17.1 at.%, exhibit strong (200) TiN reflection. As C content increases, multiorientation was observed and the diffraction peaks were shifted to a lower 2θ angle, close to the TiC phase. In addition to the main peaks of Ti(C, N), some weak peaks were detected. Most of these weak peaks can be matched to TiO_2 brookite phase (Fig. 1), which is in line with the oxygen content measured from the coatings (Table I).

TABLE I. Compositions and hardness of the Ti–Si–C–N coatings.

Sample no.	CH_4 flow rate (mL/min)	Ti (at.%)	Si (at.%)	C (at.%)	N (at.%)	Cl (at.%)	O (at.%)	Hardness (GPa)
1	320	39.4	4.7	38.6	13.4	2.2	1.7	48
2	280	45.0	3.0	29.1	16.1	3.4	3.4	43
3	240	43.5	3.7	25.2	23.2	2.8	1.6	41
4	180	40.5	3.3	21.4	28.3	3.3	4.2	36
5	140	44.8	3.9	17.1	29.6	2.5	3.1	34
6	100	40.8	3.1	14.0	34.5	1.9	4.7	32
7	60	40.1	4.2	10.2	38.5	2.1	4.9	31

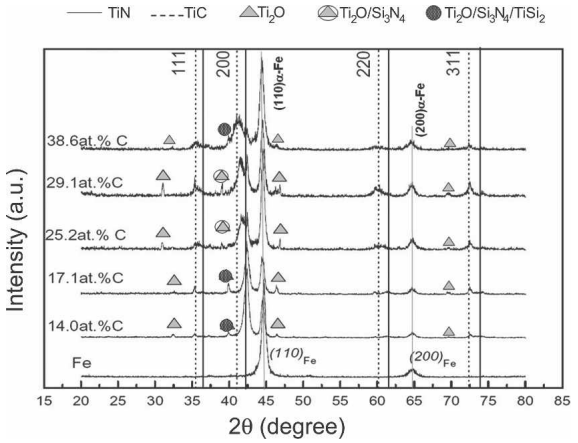

FIG. 1. XRD patterns of Ti–Si–C–N coatings with different C contents.

However, no XRD peaks, strong or weak, can be matched to TiSi, SiC, or Si_3N_4 with any degree of certainty. This is probably because of their low quantities and nano size, thus leading to few very weak XRD peaks; unfortunately, the only peaks which might be assigned to these minor phases between 2θ 39–40° are overlapped with peaks of TiO_2. Therefore, detailed TEM studies were conducted to exclusively identify these minor phases.

C. TEM characterization

Figure 2 presents TEM microstructure and corresponding selected-area electron diffraction (SAED) pattern of the coating with 17.1 at.% carbon. TEM observation of this coating revealed a multigrain structure with grain size varying from 15 to 30 nm. The dominant phase of the coating is Ti(C, N) with a face-centered-cubic (fcc) structure as indexed in Fig. 2(b). A set of weak rings can be assigned to $TiSi_2$ phase (PDF no. 35-0785, orthorhombic).[16] The (101) ring of TiO_2 phase was identified from SAED pattern, which is due to surface oxidation of sample.

The TEM microstructure and SAED pattern for coating with 25.2 at.% C are shown in Fig. 3. The coating has a very fine and uniform nanocrystallite with grain size of 10–15 nm. The SAED pattern analysis revealed that the coating consists of Ti(C, N) and Si_3N_4 (PDF No. 33-1160,[16] hexagonal) as indexed in Fig. 3(b). The continuous strong Ti(C, N) rings indicate a high-volume fraction of this phase in the coating. The TEM dark-field image in Fig. 3(c), taken from (220) Si_3N_4 rings, as indicated in Fig. 3(b), shows extremely fine nanocrystallites (8–10 nm) of Si_3N_4 dispersed uniformly in the main phase matrix. It is interesting to note that no (111) ring of Ti(C, N) could be found, indicative of a preferred orientation of (200) plane perpendicular to the specimen surface.

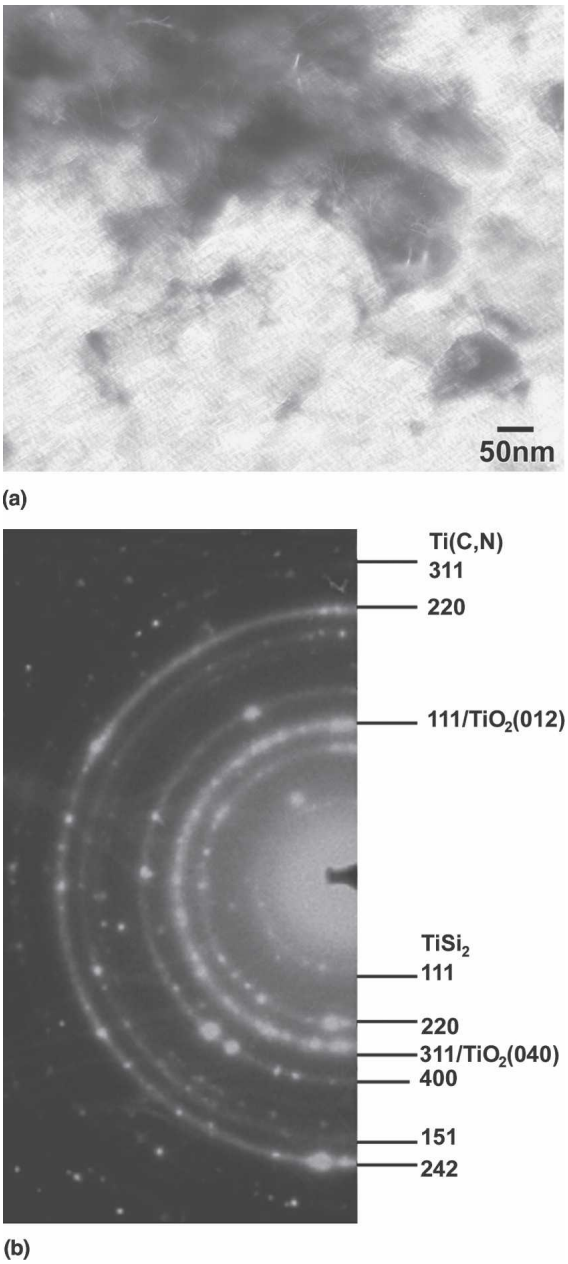

FIG. 2. (a) Bright-field TEM microstructure and (b) corresponding SAED pattern of as-deposited Ti–Si–C–N coatings with carbon content of 17.1 at.%.

As shown in Fig. 4, TEM observations of the coating with 38.6 at.% C revealed extremely fine (8–10 nm) nanocrystallites. Corresponding selected-area diffraction (SAD) pattern [Fig. 4(b)] showed that there are two sets of diffraction rings superimposed, which can be indexed to the Ti(CN) and SiC (PDF No. 29-1131, hexagonal)[16] phases. The dark-field image of Fig. 4(c), taken by part of the (0012) SiC ring, indicates the sizes of SiC particles in the coating are very fine (6–8 nm) and distributed evenly on the dominant Ti(C, N) phase. It was noted that no (111) and (311) rings of Ti(CN) could be detected,

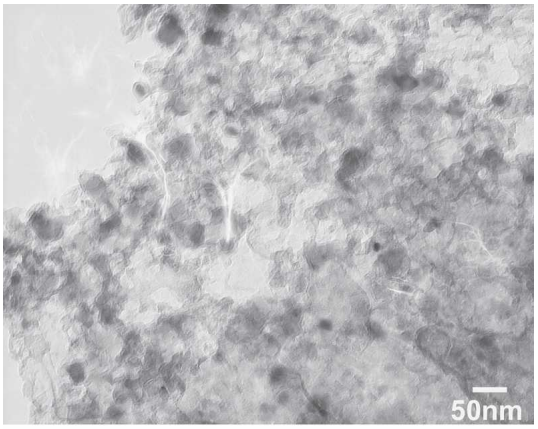

(a)

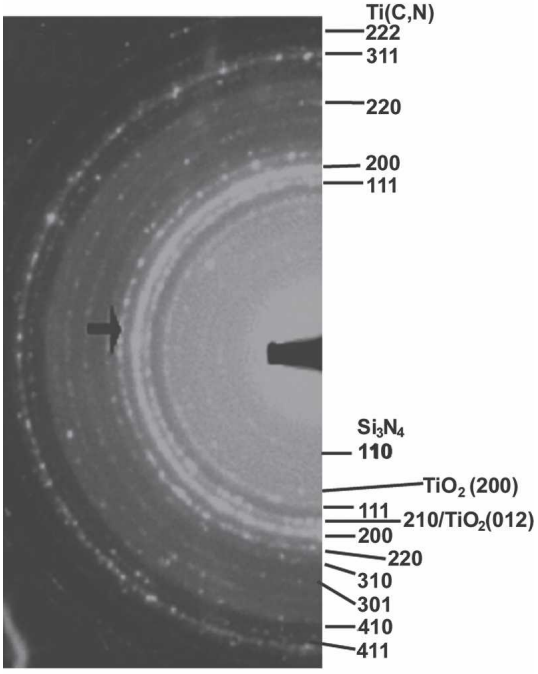

(b)

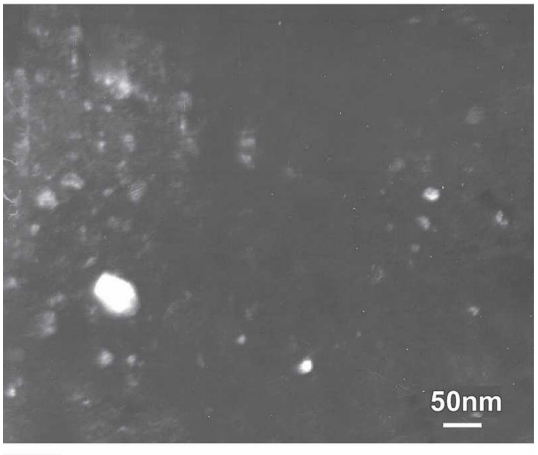

(c)

FIG. 3. (a) TEM microstructure, (b) corresponding SAED pattern, and (c) dark-field image taken from Si_3N_4 rings [as shown by the arrow in (b)] of as-deposited Ti–Si–C–N coatings with carbon content of 25.2 at.%.

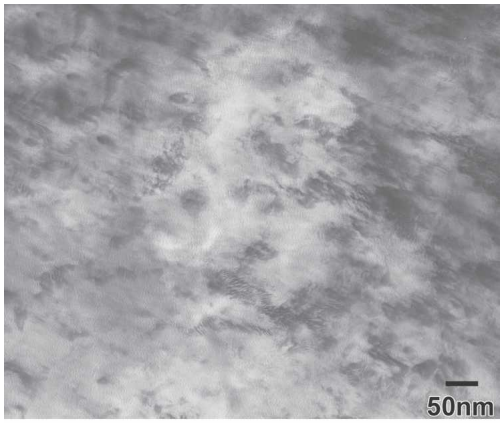

(a)

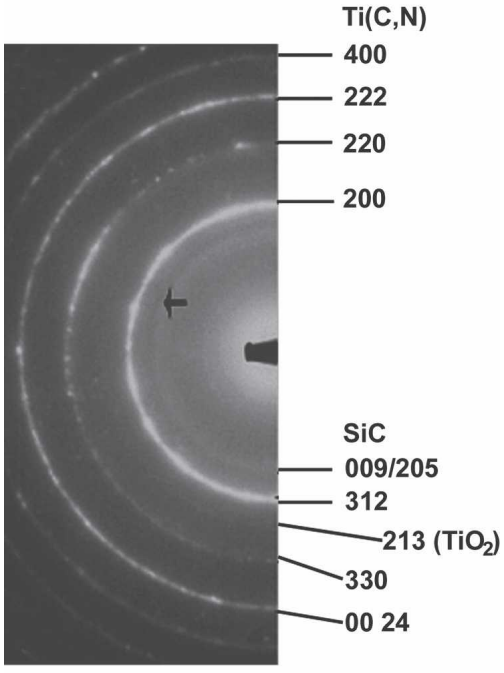

(b)

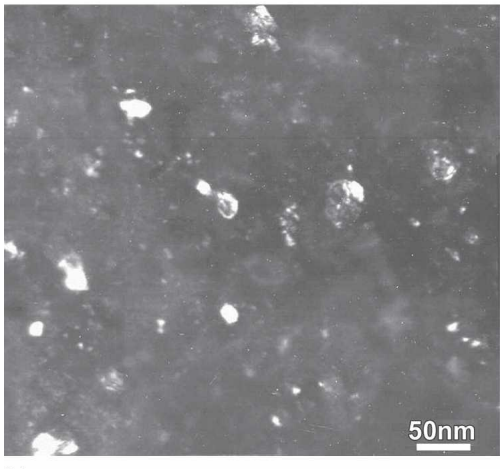

(c)

FIG. 4. (a) TEM microstructure, (b) corresponding SAED pattern, and (c) dark-field image taken from SiC rings [as shown by the arrow in (b)] of as-deposited Ti–Si–C–N coatings with carbon content of 38.6 at.%.

indicating a preferred orientation of (200) plane perpendicular to the specimen surface.

D. Hardness

As shown in Table I, the hardness of the Ti–Si–C–N coating developed from the research ranges from 31 to 48 GPa. Fig. 5 illustrates that the hardness of Ti–Si–C–N coatings increased linearly with the increase in C content, whereas the crystallite size showed an opposite way with increasing C content. For example, the hardness reached the maximum value of approximately 48 GPa when the crystallite size reached the minimum value of approximately 8 nm at the C content of 38.6 at.%. Therefore, the superhardness of these nanocomposite coatings can be attributed to the nano-scale grains size as predicted by the well-known Hall–Petch equation. The formation of small grain sizes gave rise to a high density of grain boundaries. Increasing grain boundaries can diminish dislocation activity, thus resulting in grain boundary hardening. This is because the deformation begins with the motion of dislocations that can interact with each other and impinge on the grain boundary,[17,18] and the grain boundary can accommodate many dislocations before it responds. The decrease in dislocation activity caused by the grain boundary is supported by the fact that the hardness at the grain boundary is higher than that at the grain interior.[19,20]

The grain refining effect conferred by increasing CH_4 flow rate and thus the carbon content could be related to the formation of extremely fine carbides and nitrides. It is well known that Si_3N_4 and SiC are strong, creep-resistant ceramics with outstanding mechanical properties,[21] such as high hardness of 21.0 GPa[22] and 25–31 GPa,[23] respectively. When C content is high (≥25.2 at.%), the hardness of Ti–Si–C–N coatings containing these fine, reinforced ceramics (see Figs. 3 and 4) reached superhardness values, in the range of 41–48 GPa (see Table I). It is likely that the uniform dispersion of the fine Si_3N_4 and SiC ceramic phases with high hardness (21.0–31.0 GPa) within the main-phase Ti(C, N) matrix [see Figs. 3(c) and 4(c)] may have effectively stopped the growth of Ti(C, N) grains, thus leading to nanoscale composite. In addition, the uniform dispersion of the fine Si_3N_4 and SiC ceramic phases also could, to some extent, contribute to particle (dispersion) strengthening.

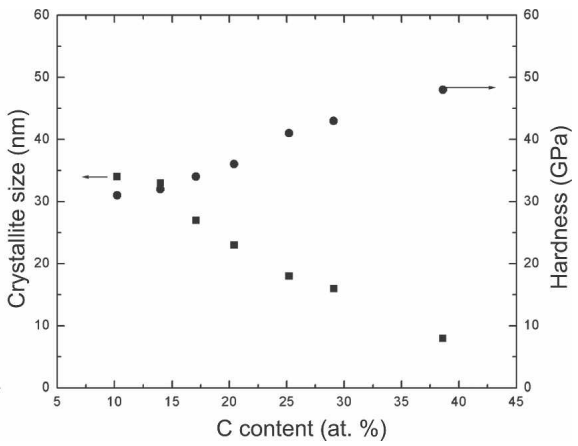

FIG. 5. Effect of C content on the crystallite size and hardness of Ti–Si–C–N coating.

IV. CONCLUSIONS

The following conclusions can be drawn based on the above experimental results and discussion:

(1) The XRD patterns from the PECVD deposited Ti–Si–C–N coatings are characterized by peak broadening and incompatible peak shift, which is mainly caused by the formation of nanoscale grains.

(2) TEM studies reveal that the synthesized nanocomposite coatings consist of dominate nano-scaled (10–30 nm) Ti(C, N) crystallites together with nano-sized (6–10 nm) crystalline secondary phases $TiSi_2$, Si_3N_4, or SiC, depending on carbon content in the coatings.

(3) The hardness of the Ti–Si–C–N coatings ranging from 31 to 48 GPa is mainly determined by their grain size. The superhardness (>40 GPa) of the high-carbon (>25.2 at.% C) coatings can be attributed to the grain refinement/grain boundary hardening and dispersion hardening of the hard, nano-sized crystalline Si_3N_4 or SiC formed during the deposition process.

ACKNOWLEDGMENTS

The authors are grateful for the financial support provided by the National Science Foundation of China (No. 50671079), the International Key Joint Project of National Science Foundation of China (50420130033), National Key Basic Research Program of China (2004CB619302), Program for New Century Excellent Talents in University of China (NCET-04-0934), Doctorate Foundation of Xi'an Jiaotong University (X020-082062), and Research Program fellowship of Xi'an Jiaotong University.

One of the authors (Yan Guo) is grateful to assistance of staff and students in the Surface Engineering Group, Department of Metallurgy and Materials at the University of Birmingham, United Kingdom.

REFERENCES

1. S. Ma, D. Ma, K. Xu, and W. Jie: Structural characterization of nanocomposite Ti–Si–N coatings prepared by pulsed dc plasma-enhanced chemical vapor deposition. *J. Vac. Sci. Technol., B* **22,** 1694 (2004).
2. Y. Guo, S. Ma, and K. Xu: Effects of carbon content and annealing temperature on the microstructure and hardness of super hard

Ti–Si–C–N nanocomposite coatings prepared by pulsed d.c. PCVD. *Surf. Coat. Technol.* **210,** 5240 (2007).
3. M. Wittmer, J. Noser, and H. Melchior: Oxidation kinetics of TiN thin films. *J. Appl. Phys.* **52**(11), 6659 (1981).
4. J-W. He, C-D. Bai, K-W. Xu, and N-S. Hu: Improving the anti-corrosion and mechanical behaviour of PACVD TiN. *Surf. Coat. Technol.* **74–75,** 387 (1995).
5. X.Z. Ding, X.T. Zeng, Y.C. Liu, Q. Yang, and L.R. Zhao: Structure and mechanical properties of Ti–Si–N films deposited by combined DC/RF reactive unbalanced magnetron sputtering. *J. Vac. Sci. Technol., A* **22,** 2351 (2004).
6. J. Bujak, J. Walkowicza, and J. Kusiński: Influence of the nitrogen pressure on the structure and properties of (Ti,Al)N coatings deposited by cathodic vacuum arc PVD process. *Surf. Coat. Technol.* **180–181,** 150 (2004).
7. P. Karvánková, M.G.J. Vepřek-Heijman, M.F. Zawrah, and S. Vepřek: Thermal stability of nc-TiN/a-BN/a-TiB_2 nanocomposite coatings deposited by plasma chemical vapor deposition. *Thin Solid Films* **467,** 133 (2004).
8. Y. Otani and S. Hofmann: High temperature oxidation behavior of $(Ti_{1-x}Cr_x)N$ coatings. *Thin Solid Films* **287,** 188 (1996).
9. X. Hu, H. Zhang, J. Dai, G. Li, and M. Gu: Study on the superhardness mechanism of Ti–Si–N nanocomposite films: Influence of the thickness of the Si_3N_4 interfacial phase. *J. Vac. Sci. Technol., A* **23,** 114 (2005).
10. S. Veprek and S. Reiprich: A concept for the design of novel superhard coatings. *Thin Solid Films* **268,** 64 (1995).
11. S. Hofmann: Formation and diffusion properties of oxide films on metals and on nitride coatings studied with Auger electron spectroscopy and x-ray photoelectron spectroscopy. *Thin Solid Films* **193–194,** 648 (1990).
12. O-N. Park, J.H. Park, S-Y. Yoon, M-H. Lee, and K.H. Kim: Tribological behavior of Ti–Si–N coating layers prepared by a hybrid system of arc ion plating and sputtering techniques. *Surf. Coat. Technol.* **179,** 83 (2004).
13. A. García-Luis, T.M. Brizuela, J.I. Oñate, J.C. Sánchez-López, D. Martínez-Martínez, C. López-Cartes, and A. Fernández: Mechanical properties of nanocrystalline Ti–B–(N) coatings produced by DC magnetron sputtering. *Surf. Coat. Technol.* **200,** 734 (2005).
14. J-H. Jeon, S.R. Choi, W.S. Chung, and K.H. Kim: Synthesis and characterization of quaternary Ti–Si–C–N coatings prepared by a hybrid deposition technique. *Surf. Coat. Technol.* **188–189,** 415 (2004).
15. J. Musil: Hard and superhard nanocomposite coatings. *Surf. Coat. Technol.* **125,** 322 (2000).
16. PDF Nos. 35-0785, 33-1160, and 29-1131. International Center for Diffraction Data: Newton Square, PA, 1999.
17. G.M. Bond, I.M. Roberton, and H.K. Birnbaum: Effect of boron on the mechanism of strain transfer across grain boundaries in Ni_3Al. *J. Mater. Res.* **2,** 436 (1987).
18. Z-J. Liu, P.W. Shum, and Y.G. Shen: Hardening mechanisms of nanocrystalline Ti–Al–N solid solution films. *Thin Solid Films* **468,** 161 (2004).
19. A. Lasalmonie and J.L. Strudel: Influence of grain size on the mechanical behavior of some high strength materials. *J. Mater. Sci.* **21,** 1837 (1986).
20. R.A. Masumura, P.M. Hazzledine, and C.S. Pande: Yield stress of fine grained materials. *Acta Mater.* **46,** 4527 (1998).
21. S.M. Wiederhorn, B.J. Hockey, and J.D. French: Mechanisms of deformation of silicon nitride and silicon carbide at high temperatures. *J. Eur. Ceram. Soc.* **19,** 2273 (1999).
22. S. Ogata, N. Hirosaki, C. Kocer, and Y. Shibutal: A comparative ab initio study of the "ideal" strength of single crystal α- and β-Si_3N_4. *Acta Mater.* **52,** 233 (2004).
23. O. Borrero-López, A. Pajares, A.L. Ortiz, and F. Guiberteau: Hardness degradation in liquid-phase-sintered SiC with prolonged sintering. *J. Eur. Ceram. Soc.* **27,** 3359 (2007).